Hexamethylenetetramine mediated 1 simultaneous nitrogen doping and reduction of graphene oxide for a metal-free SERS substrate

ARTICLE *in* RSC ADVANCES · AUGUST 2014

Impact Factor: 3.84 · DOI: 10.1039/c4ra08787a

1 AUTHOR:

Barun Barman
Indian Institute of Science
8 PUBLICATIONS **38** CITATIONS

RSC Advances

COMMUNICATION

View Article Online
View Journal | View Issue

Cite this: *RSC Adv.*, 2014, **4**, 44146

Hexamethylenetetramine mediated simultaneous nitrogen doping and reduction of graphene oxide for a metal-free SERS substrate†

Barun Kumar Barman and Karuna Kar Nanda*

Received 11th July 2014
Accepted 28th August 2014

DOI: 10.1039/c4ra08787a

www.rsc.org/advances

We report a one-pot hydrothermal synthesis of nitrogen doped reduced graphene oxide (N-rGO) and Ag nanoparticle decorated N-rGO hybrid nanostructures from graphene oxide (GO), metal ions and hexamethylenetetramine (HMT). HMT not only reduces GO and metal ions simultaneously but also acts as the source for the nitrogen (N) dopant. We show that the N-rGO can be used as a metal-free surface enhanced Raman spectroscopy (SERS) substrate, while the Ag nanoparticles decorated N-rGO can be used as an effective SERS substrate as well as a template for decorating various other nanostructures on N-rGO.

Pristine, doped and nanoparticle (NP) decorated graphenes have gained great attention due to their extraordinary electronic, mechanical and thermal properties and their applications in various fields such as electronics, optical sensors, energy storage applications, *etc.*[1] The performance is shown to be improved significantly when the graphene is modified by doping[2,3] or decorating with metal NPs.[4] For example, nitrogen doped graphene[5] and graphene decorated with metal/metal oxide NPs[6] can be an excellent catalyst for oxygen reduction reaction[7] and metal decorated graphene can be used for surface enhanced Raman spectroscopy (SERS),[8–11] reduction of nitrophenol,[12,13] *etc.* The synthesis of doped and metal NPs decorated graphene with good control of size and structures is of paramount importance for specific applications. However, it is a challenge to synthesize nitrogen doped graphene or graphene decorated with metal NPs in large scale. Though several approaches such as micromechanical exfoliation of graphite,[14] chemical vapour deposition (CVD),[15] and epitaxial growth,[16] chemical reduction of graphene oxide (GO) to obtain reduced graphene oxide (rGO),[17–19] has the advantage of large scale production and cost effective. Similarly, simultaneous reduction and decoration of metal NPs is the most viable approach for the large scale synthesis of the hybrids. Simultaneous reduction of GO and nitrogen doping has also been achieved by heating GO in presence of ammonia,[20] chemical vapour deposition,[21,22] and hydrothermal and method.[20–24]

Here, we report the one-step synthesis of nitrogen doped rGO (N-rGO) and Ag NPs/N-rGO hybrids from GO by using hexamethylenetetramine (HMT). HMT acts as a reducing agent for both GO and Ag^+ ions and N source for doping. The overall chemical reactions are presented in Fig. 1. We show that the N-rGO can be used as metal-free SERS substrates and SERS can further be enhanced by the presence of Ag NPs. We also show that the Ag NPs/N-rGO hybrid nanostructures can be used as effective template for decorating porous metallic nanostructures on N-rGO.

In order to synthesize N-rGO, GO flakes along with HMT solution was taken in an autoclave and treated at 180 °C for 10 h in absence of any surfactant and reducing agent. We chose HMT ($(CH_2)_6N_4$) for this reaction, which is a water-soluble, nontoxic, non-ionic and tetradentate cyclic ternary amine.[22] In aqueous medium, it releases hydroxyl ion, ammonia (NH_3) and formaldehyde (HCHO). As a result GO gets reduced and doped by N simultaneously in presence of HCHO and NH_3, respectively and finely we are getting black precipitation of N-rGO. Similarly, Ag

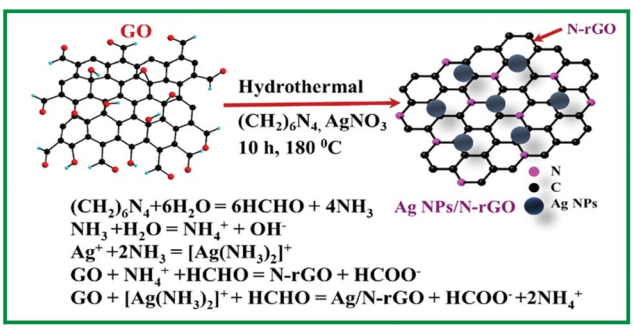

Fig. 1 Schematic diagram and chemical equation of for Ag/N-rGO hybrids nanostructures by simultaneous reduction of both Ag^+ ions and GO followed by N doping in rGO.

Materials Research Centre, Indian Institute of Science, Bangalore-560012, India. E-mail: nanda@mrc.iisc.ernet.in; Fax: +91 80 2360 7316; Tel: +91 80 2293 2996

† Electronic supplementary information (ESI) available. See DOI: 10.1039/c4ra08787a

NPs/N-rGO were obtained by taking GO, HMT and $AgNO_3$. When Ag^+ ions are added, it formed 2-coordinate Ag(I) complex with the NH_3. This complex can be further reduced by HCHO in the reaction medium to form Ag NPs on the graphene sheet. The entire results suggest that HMT plays multiple roles in the reaction medium and the overall reaction for the one-step synthesis of Ag NPs/N-rGO are provided in schematic Fig. 1. We also decorated Pd nanostructures on N-rGO substrate by sacrificing Ag NPs by galvanic replacement reaction (GRR).

Fig. 2A & B show of SEM images of crumbled solid N-rGO and dense Ag NPs decorated N-rGO sheet. We have performed few more experiments in order to control the size and the density of the Ag NPs. When the Ag^+ ions concentration in the reaction mixture is reduced, the density of Ag NPs gradually decreases and the size of the NPs increases on randomly aggregated, crumpled solid sheets as shown in ESI-1.† Fig. 2C & D display the TEM images of GO and N-rGO sheet and the inset images display the corresponding SAED patterns. Transformation from the ring-like pattern of GO to clear individual spot in the SEAD pattern of N-rGO suggests the reduction GO. The loss of oxygen containing functional group helps to regain the crystalline graphitic nature in N-RGO from the polycrystalline nature of GO.[25] The size of Ag NPs as obtained from TEM image (Fig. 2E) is in 16–26 nm range and the average diameter is ~22 nm. The *d*-spacing is 0.235 nm of Ag NPs is calculated from Fig. 2F and single crystalline as confirmed from the SAED pattern[26,27] Hereafter, the sample with ~22 nm Ag NPs is referred as Ag(h)/N-rGO and the results are mainly presented for this sample. For another case, the average size of the Ag NPs is ~70 nm and is referred to Ag(l)/N-rGO.

The N-rGO sheets decorated with Ag NPs are characterized by XRD. XRD patterns shown in Fig. 3A reveal five intense peaks at $2\theta = 38°$, 44.25°, 64.5°, 77.26° and 81.54°, which are assigned to (111), (200), (220), (311) and (222) planes of Ag (JCPDS no. 04-0783). Generally, GO shows a sharp peak at around $2\theta = 11.5°$, which corresponds to *d*-spacing of 0.76 nm for (001) plane due to the presence of oxygen functionalities. The sharp peak corresponding to GO is absent and a broad peak appears at values $2\theta = 24.5$ degree which is assigned to (002) plane of rGO (ESI-2†). The *d*-spacing is estimated to be 0.36 nm which suggests the removal of large number of oxygen and functional group from GO (ESI†). Overall, the results confirm the presence of Ag NPs in face-centered cubic (fcc) phase on N-rGO sheets. The reduction of GO and presence of Ag NPs is also confirmed by UV-visible spectroscopy as shown in Fig. 3B. In general, GO displays a strong peaks at 230 nm, corresponding to π–π* transitions of aromatic C–C bonds, and a weak peaks around 300 nm due to n–π* transitions of C=O bonds. The 230 nm peak is red shifted to 266 nm indicating the electronic conjugation within graphene sheet is recovered after reduction of GO.[28–31] A broad peak around 420 nm appeared for Ag(l)/N-rGO. This is the characteristic absorption peak of Ag NPs due to the surface plasmon resonance (SPR). When we increase the amount of Ag NPs on the graphene surface, the intensity of the SPR peak at ~420 nm increased with a slight blue-shift of 4 nm which is in accordance with other reports.[32,33]

XPS studies are carried out to determine the elemental composition along with their chemical state and also intuitively estimate the reduction level of GO and doping of N. Fig. 4A presents the survey XPS spectra of GO, N-rGO and Ag NPs/N-rGO hybrids. It can be noted for N-rGO that the peak corresponding to C1s increases confirming the reduction of GO. Furthermore, a peak corresponding to N1s appears that confirm the doping of N. Similarly, reduction, doping and the formation of Ag NPs is realized from the XPS spectrum of Ag NPs/N-rGO. In order to estimate the reduction rate of GO, the C1s spectra (Fig. 4B) were deconvoluted into three major peaks with the binding energy 284.5, 285.8 and 287.6 eV that corresponds to C–C/C=C (sp^2/sp^3 bonding energy of carbon), C–O (epoxy, alcohol, ester and acid groups) and C=O (carbonyl groups), respectively. The most prominent peak corresponds to C–C (284.6 eV). The percentage of reduction were calculated by the area under the following

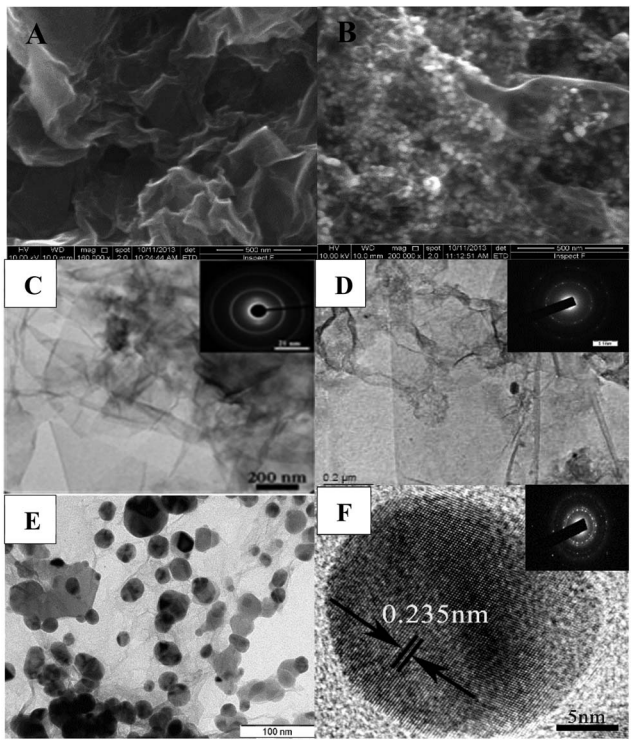

Fig. 2 (A & B) SEM images of N-rGO and Ag(h)/N-rGO nanostructures. (C &D) TEM images GO and N-rGO (inset images corresponding to the SAED pattern). (C and D) represent the TEM and HRTEM images of Ag(h)/N-rGO hybrids.

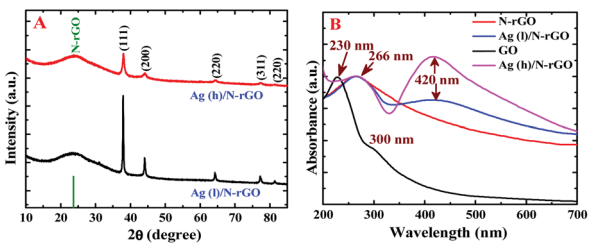

Fig. 3 (A & B) XRD and UV-vis absorption spectra of hybrids.

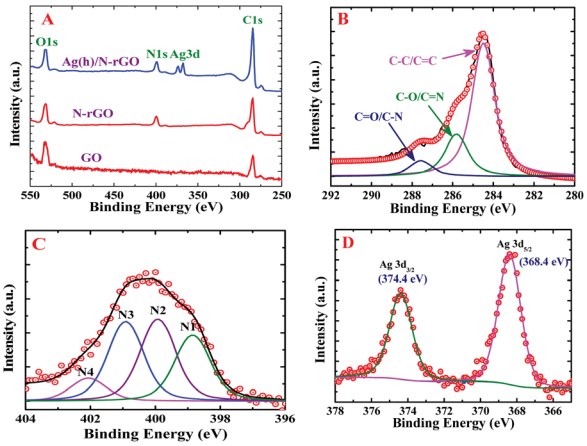

Fig. 4 (A) XPS survey of GO, N-rGO and Ag(h)/N-rGO & spectra of (B) C1s, (C) N1s and (D) Ag3d of Ag(h)/N-rGO sample.

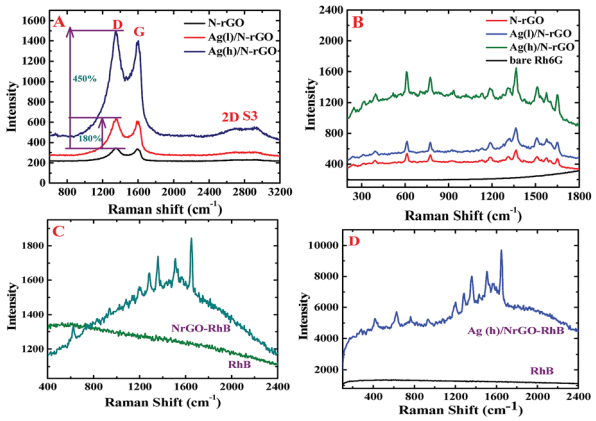

Fig. 5 (A) The presence of Ag NPs enhances the native Raman spectra of N-rGO sheets by 180 and 450%, characteristic for a chemical enhancement of N-rGO substrate. (B) Raman spectra of different hybrids nanostructures in presence of 100 μM Rh6G probe molecule. (C & D) Raman spectra of RhB (100 μM) in presence of N-rGO and Ag(h)/N-rGO substrate. All samples are coated on soda lime glass.

three curves in C1s spectra and amount of the C–C bonds increases from 30% to ~70%, while the C–O and C=O bonds decreases from 50.6% to ~22% and 19.4% to ~8%, respectively. The doping of N was also confirmed by XPS. The binding energies of C–O and C–N bonds are very close and therefore, it is difficult to deconvolute the C1s spectra of N-rGO. However, the deconvolution of the high resolution XPS of N1s spectrum as shown in Fig. 4C yields four major peaks that correspond to pyridinic N (N1 = 398.7 eV), pyrrolic N (N2 = 400 eV), quaternary N (N3 = 401 eV) and N oxides of pyridinic N (N4 = 402.3 eV).[7,23] The area under the two peaks N1s and C1s is used to determine the percentage of N doping which also correlated with the energy dispersive X-ray spectra (ESI-3,† Fig. 3 & 4). We can see that ~11% N was doped in rGO. Fig. 4D represents the Ag3d doublet of Ag NPs, where two bands at 368.4 eV and 374.4 eV are attributed to the binding energy of $Ag3d_{5/2}$ and $Ag3d_{3/2}$ electronic states, respectively. These two binding energy values are fairly higher than the of Ag metallic Ag (0), where this two energy states appear at 367.9 and 373.9 eV.[34,35] These 0.5 eV higher binding energy shift can be described by the electron transfer from Ag NPs to rGO in the hybrids due to the lower work function of rGO (>4.8 eV) compared to Ag (4.2 eV). The purity of metallic Ag in the form of NPs was also confirmed by the 6 eV energy difference between the doublets of Ag3d electronic states.[36]

The reduction of GO to N-rGO is also probed by micro Raman analysis (ESI-4†). Both the GO and N-rGO are containing two major peak centred 1351 (A_{1g} vibrational mode, D band) and 1589 cm^{-1} (E_{2g} vibrational mode, G band). The D band arises due to the defect and G peak corresponding to the graphitic peak. After the reduction of GO, the I_D/I_G intensity ratio slightly increases from 0.96 to 1.02 confirming the reduction of GO. The interaction of Ag NPs with N-rGO is further probed by SERS. The SERS can be achieved *via* two main reasons: (i) electromagnetic enhancement which is arise due to the SPR by physical interaction and (ii) chemical enhancement due to the formation of charge transfer complex *via* chemical bonding. It is interesting to note from Fig. 5A that the peak intensity of both the D and G band are enhanced by 180% (1.8 fold) and 450% (4.5 fold) when decorated with the Ag(l) and Ag(h) NPs. Overall, the enhancement factor is around 450% for smaller NPs and 180% for bigger NPs. This low enhancement factor for Ag/N-rGO hybrids indicates the presence of a chemical interaction between the Ag NPs and N-rGO rather than electromagnetic enhancement.[37,38] We also probe the Raman signal for Rhodamine 6G (Rh6G) and Rhodamine B (RhB). It can be noted from Fig. 5B that peaks around 612, 776, 934, 1135, 1192, 1314, 1367, 1425, 1510, 1579 and 1652 cm^{-1} are in good agreement with earlier reports on Rh6G.[39]

Overall, though the enhancement is high for Ag(h)/N-rGO, N-rGO can also be used as metal-free SERS substrate. In the case of RhB,[40] the peaks at 624, 937, 1024, 1083, 1136, 1198, 1287, 1359, 1509, 1564 and 1650 cm^{-1} are nicely seen through both N-rGO and Ag(h)/N-rGO as shown in Fig. 5C & D, though the enhancement in the latter case is high. We have also investigated SERS of other probe molecules such as malachite green (MG) and congo red (CR) dye molecules (ESI-5†).[41] It is believed that the Fermi energy level of N-rGO (4.8 eV) lies between the HOMO and LUMO energy levels of these dye molecules which facilitates π–π bonding interaction *via* formation of charge transfer complex between the dyes and N-rGO. When for 4-marcapto benzoic acid (4-MBA) – a well-known SERS probe molecule on the metal substrate (Ag, Au *etc.*) is Raman inactive in presence of N-rGO as shown in ESI.† However, SERS is observed with Ag(h)/N-rGO as shown in ESI.† In this case, the energy difference between the HOMO (6.23 eV) – LUMO (1.29 eV) are very high around 4.94 eV which doesn't favor the π–π chemical interaction with the graphene. On the other hand, the bonding between thiol group (–SH) with the Ag is responsible for the SERS with Ag/N-rGO (ESI-Fig. 5E & F†).

We also synthesize Pd nanostructures by GRR using Ag(h)/N-rGO hybrids at room temperature. The standard reduction potential of $E_{Ag^+/Ag}$ and $E_{Pd^{2+}/Pd}$ is 0.80 and 0.90 V *vs.* standard electrode respectively. When Pd^{2+} ions are introduced into the

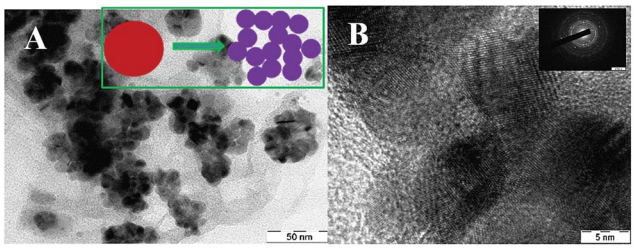

Fig. 6 (A) shows the porous Pd nanostructures on N-rGO substrate by using Ag(h)/N-rGO as templates (inset shows the schematic of the Pd nanostructures) and (B) shows the HRTEM images of ligand of the porous Pd (Inset images shows the SAED pattern).

hybrid solution, Pd nanostructures are obtained by sacrificing Ag NPs on N-rGO by following this chemical eqn Ag/N-rGO + Pd^{2+} → Pd/N-rGO + Ag^{+}. This is well supported by UV-vis and Raman spectroscopy (ESI-6†). TEM and HRTEM images (Fig. 6A & B) clearly confirm the porous structures of Pd which is larger than the size of the Ag NPs.

In conclusion, we report a one-step hydrothermal method for the synthesis of N-rGO and metal NPs decorated N-rGO hybrid nanostructures from GO, metal ions and HMT. The roles of HMT are to reduce the GO, the metal ions and the nitrogen source for doping rGO. We show that N-rGO as metal-free SERS substrate for the detection of various dyes molecules *via* chemical interaction. We also show that the hybrid nanostructures can be used as effective SERS substrate and template for decorating other various metallic nanostructures on N-rGO.

Notes and references

1 Y. Zhu, S. Murali, W. Cai, X. Li, J. W. Suk, J. R. Potts and R. S. Ruoff, *Adv. Mater.*, 2010, **22**, 3906–3924.
2 I. Y. Jeon, D. Yu, S. Y. Bae, J. H. Choi, D. W. Chang, L. Dai and J. B. Baek, *Chem. Mater.*, 2011, **23**, 3987–3992.
3 (*a*) H. Sun, Y. Wang, S. Liu, L. Ge, L. Wang, Z. Zhu and S. Wang, *Chem. Commun.*, 2013, **49**, 9914–9916; (*b*) D. Deng, X. Pan, L. Yu, Y. Cui, Y. Jiang, J. Qi, W. X. Li, Q. Fu, X. Ma, Q. Xue, G. Sun and X. Bao, *Chem. Mater.*, 2011, **23**, 1188–1193.
4 X. K. Kong, C. L. Chen and Q. W. Chen, *Chem. Soc. Rev.*, 2014, **43**, 2841.
5 L. Qu, Y. Liu, J. B. Baek and L. Dai, *ACS Nano*, 2010, **4**, 1321–1326.
6 Y. Liang, Y. Li, H. Wang, J. Zhou, J. Wang, T. Regier and H. Dai, *Nat. Mater.*, 2011, **10**, 780–786.
7 Y. Shao, S. Zhang, M. H. Engelhard, G. Li, G. Shao, Y. Wang, J. Liu, I. A. Aksay and Y. Lin, *J. Mater. Chem.*, 2010, **20**, 7491–7496.
8 X. Ling, L. Xie, Y. Fang, H. Xu, H. Zhang, J. Kong, M. S. Dresselhaus, J. Zhang and Z. Liu, *Nano Lett.*, 2009, **10**, 553–561.
9 W. Xu, N. Mao and J. Zhang, *Small*, 2013, **9**, 1206–1224.
10 W. Xu, X. Ling, J. Xiao, M. S. Dresselhaus, J. Kong, H. Xu, Z. Liu and J. Zhang, *Proc. Natl. Acad. Sci. U. S. A.*, 2012, **109**, 9281–9286.
11 W. Xu, J. Xiao, Y. Chen, Y. Chen, X. Ling and J. Zhang, *Adv. Mater.*, 2013, **25**, 928–933.
12 X. K. Kong, Z. Y. Sun, M. Chen, C. L. Chen and Q. W. Chen, *Energy Environ. Sci.*, 2013, **6**, 3260–3266.
13 H. K. Sadhanala, J. Khatei and K. K. Nanda, *RSC Adv.*, 2014, **4**, 11481–11485.
14 K. S. Novoselov, A. K. Geim, S. V. Morozov, D. Jiang, Y. Zhang, S. V. Dubonos, I. V. Grigorieva and A. A. Firsov, *Science*, 2004, **306**, 666–669.
15 K. S. Kim, Y. Zhao, H. Jang, S. Y. Lee, J. M. Kim, K. S. Kim, J. H. Ahn, P. Kim, J. Y. Choi and B. H. Hong, *Nature*, 2009, **457**, 706–710.
16 P. W. Sutter, J. I. Flege and E. A. Sutter, *Nat. Mater.*, 2008, **7**, 406–411.
17 S. Stankovich, D. A. Dikin, R. D. Piner, K. A. Kohlhaas, A. Kleinhammes, Y. Jia, Y. Wu, S. T. Nguyen and R. S. Ruoff, *Carbon*, 2007, **45**, 1558–1565.
18 S. Park and R. S. Ruoff, *Nat. Nanotechnol.*, 2009, **4**, 217–224.
19 V. C. Tung, M. J. Allen, Y. Yang and R. B. Kaner, *Nat. Nanotechnol.*, 2009, **4**, 25–29.
20 X. Li, H. Wang, J. T. Robinson, H. Sanchez, G. Diankov and H. Dai, *J. Am. Chem. Soc.*, 2009, **131**, 15939–15944.
21 Z. Jin, J. Yao, C. Kittrell and J. M. Tour, *ACS Nano*, 2011, **5**, 4112–4117.
22 (*a*) J. W. Lee, J. M. Ko and J. D. Kim, *Electrochim. Acta*, 2012, **85**, 459–466; (*b*) X. Shen, L. Jiang, Z. Ji, J. Wu, H. Zhou and G. Zhu, *J. Colloid Interface Sci.*, 2011, **354**, 493–497.
23 (*a*) S. Maldonado, S. Morin and K. J. Stevenson, *Carbon*, 2006, **44**, 1429–1437; (*b*) H. Wang, T. Maiyalagan and X. Wang, *ACS Catal.*, 2012, **2**, 781–794; (*c*) Z. H. Sheng, L. Shao, J. J. Chen, W. J. Bao, F. B. Wang and X. H. Xia, *ACS Nano*, 2011, **5**, 4350–4358.
24 (*a*) L. Sun, L. Wang, C. Tian, T. Tan, Y. Xie, K. Shi, M. Li and H. Fu, *RSC Adv.*, 2012, **2**, 4498–4506; (*b*) D. Yu, J. Yao, L. Qiu, Y. Wu, L. Li, Y. Feng, Q. Liu, D. Lic and H. Wang, *RSC Adv.*, 2013, **3**, 11552–11555; (*c*) Z. Lin, M. K. Song, Y. Ding, Y. Liu, M. Liu and C. P. Wong, *Phys. Chem. Chem. Phys.*, 2012, **14**, 3381–3387.
25 E. Yoo, J. Kim, E. Hosono, H. Zhou, T. Kudo and I. Honma, *Nano Lett.*, 2008, **8**, 2277–2282.
26 j. Tian, S. Liu, Y. Zhang, H. Li, L. Wang, Y. Luo, A. M. Asiri, A. O. Al-Youbi and X. Sun, *Inorg. Chem.*, 2012, **51**, 4742–4746.
27 Z. Zhang, F. Xu, W. Yang, M. Guo, X. Wang, B. Zhang and J. Tang, *Chem. Commun.*, 2011, **47**, 6440–6442.
28 Z. Fan, K. Wang, T. Wei, J. Yan, L. Song and B. Shao, *Carbon*, 2010, **48**, 1686–1689.
29 Z. J. Fan, W. Kai, J. Yan, T. Wei, L. J. Zhi, J. Feng, Y. M. Ren, L. P. Song and F. Wei, *ACS Nano*, 2010, **5**, 191–198.
30 B. K. Barman, P. Mahanandia and K. K. Nanda, *RSC Adv.*, 2013, **3**, 12621–12624.
31 Y. Zhu, W. Cai, R. D. Piner, A. Velamakanni and R. S. Ruoff, *Appl. Phys. Lett.*, 2009, **95**, 123115.
32 X. Z. Tang, Z. Cao, H. B. Zhang, J. Liu and Z. Z. Yu, *Chem. Commun.*, 2011, **47**, 3084–3086.
33 J. Li and C. Y. Liu, *Eur. J. Inorg. Chem.*, 2010, 1244–1248.

34 V. G. Pol, D. N. Srivastava, O. Palchik, V. Palchik, M. A. Slifkin, A. M. Weiss and A. Gedanken, *Langmuir*, 2002, **18**, 3352–3357.
35 T. Wu, H. Shen, L. Sun, B. Cheng, B. Liu and J. Shen, *ACS Appl. Mater. Interfaces*, 2012, **4**, 2041–2047.
36 S. Dutta, C. Ray, S. Sarkar, M. Pradhan, Y. Negishi and T. Pal, *ACS Appl. Mater. Interfaces*, 2013, **5**, 8724–8732.
37 K. Jasuja and V. Berry, *ACS Nano*, 2009, **3**, 2358–2366.
38 K. Jasuja, J. Linn, S. Melton and V. Berry, *J. Phys. Chem. Lett.*, 2010, **1**, 1853–1860.
39 (*a*) Z. Yuda, X. Yizh, B. Zhiyong, H. Yuen, T. Hong Tsang, X. Liming and C. Y. Chai, *J. Phys. Chem. C*, 2014, **118**, 11827–11832; (*b*) R. Lv, Q. Li, A. R. Botello-Méndez, T. Hayashi, B. Wang, A. Berkdemir, Q. Hao, A. L. Elías, R. Cruz-Silva and H. R. Gutiérrez, *Sci. Rep.*, 2012, **2**, 586.
40 X. Yu, H. Cai, W. Zhang, X. Li, N. Pan, Y. Luo, X. Wang and J. G. Hou, *ACS Nano*, 2011, **5**, 952–958.
41 J. Yue, M. Pinyi, L. Fanghui, G. Dejiang and W. Xinghua, *Anal. Methods*, 2013, **5**, 5609–5614.